Available online at www.sciencedirect.com

SciVerse ScienceDirect

Procedia Engineering 58 (2013) 309 – 319

Procedia Engineering

www.elsevier.com/locate/procedia

The 12th Hypervelocity Impact Symposium

Mesoscale Simulation of Mixed Equations of State with Application to Shocked Platinum-Doped PMP Foams

Thomas A. Haill[a]*, Thomas R. Mattsson[a], Seth Root[a], Rudolph J. Magyar[a], Diana G. Schroen[b]

[a]*Sandia National Laboratories, P.O. Box 5800, Albuquerque, NM 87185-1186, USA*
[b]*General Atomics, P.O. Box 85608, San Diego, CA 92186-5608*

Abstract

Hydrocarbon polymers and foams are utilized in high energy-density physics (HEDP) and inertial confinement fusion (ICF) experiments as tampers, energy conversion and radiation pulse shaping layers in dynamic hohlraum Z-pinches, and ablators in ICF capsule implosions. Shocked foams frequently are found to be mixed with other materials either by intentional doping with high-Z elements or by instabilities and turbulent mixing with surrounding materials. In this paper we present one-dimensional and three-dimensional mesoscale hydrodynamic simulations of high-Z doped poly-(4-methyl-1-pentene) (PMP or TPX) foams in order to examine the validity of various equation of state (EOS) mixing rules available in two state-of-the-art simulation codes. Platinum-doped PMP foam experiments conducted at Sandia's Z facility provide data that can be used to test EOS mixing rules. We apply Sandia's ALEGRA-MHD code and the joint LLNL/SNL KULL HEDP code to model these doped foam experiments and exercise the available EOS mixing methods. One-dimensional simulations homogenize the foam with platinum dopant and show which EOS mixing methods produce results that are consistent with measured Hugoniot states. These simulations produce sharp shock fronts that are well described by traditional Hugoniot relations. Three-dimensional mesoscale simulations explicitly model the foam structure embedded with discrete platinum particles. The heterogeneous structure of the foam results in diffuse shock fronts and an unsteady post-shock state with large fluctuations about an average state. We compare shock propagation through pure foam and Pt-doped foams (50-50 mixture by weight) at equal average initial density, and examine how well the results compare to the experimentally measured Hugoniot states.

Selection and peer-review under responsibility of the Hypervelocity Impact Society

Keywords: ALEGRA; KULL; doped foam; mesoscale simulation; equation of state; atomic mix; chunk mix

1. Introduction

Scientific and programmatic applications require mixed EOS studies to Mbar shock pressures and create a need to validate EOS mixing rules in hydrodynamics codes. For example, fuel-shell mix is observed in directly driven capsules on the Omega laser facility and up to 50% of the electron density of the imploded material is concluded to be shell material [1]. National Ignition Facility (NIF) targets have germanium-doped ablators and mixing into the ignition hot-spot due to bumps and defects in the ablator can have a significant effect on ignition capsule performance [2]. The mix of materials also affects radiative transport [3,4], conductive properties of materials [5], and multi-fluid flows [6]. Other applications include density functional theory (DFT) modeling of mixed EOS for the earth's core [7,8], the interiors of giant gas planets [9,10], and solar convection models [11]. These complex mixed systems do not always lend themselves to a precise knowledge of the relative abundance of the constituent materials, therefore simpler model systems are developed to study mixtures where the ratio of the constituents is known, such as controlled mixtures of xenon and deuterium or xenon and ethane [12,13].

* Corresponding author. Tel.: +1 505 845 7242; fax: +1 505 844 8467.
E-mail address: tahaill@sandia.gov.

Selection and peer-review under responsibility of the Hypervelocity Impact Society
doi:10.1016/j.proeng.2013.05.035

A foundation for studying the EOS of mixtures is laid by first studying the EOS of the mixture components. The least well-known component here is the poly-(4-methyl-1-pentene) (PMP or TPX) polymer from which the platinum-doped foam is manufactured. Thus, the principal Hugoniot and the molecular dissociation of polymer chains for polyethylene and PMP were previously examined using DFT and classical molecular dynamics (MD) methods [14,15]. Our prior work also studied shocked pure PMP foams, examining the Hugoniot state in the Mbar regime using experiment, hydrodynamic simulation, and classical MD simulation [16,17,18]. That study demonstrated the consistency of simulation methods over several orders of magnitude in spatial scales and laid a solid foundation to study mixed materials and mixed EOS.

In this paper we report on hydrodynamic mesoscale simulations of another model system, namely shocked platinum-doped PMP foams (50-50 mixture by weight). We apply Sandia's ALEGRA MHD code [19,20] and the joint LLNL/SNL KULL HEDP code [21] to model these doped foam experiments and exercise the available EOS mixing rules. One-dimensional simulations homogenize the foam with platinum dopant and show which EOS mixing methods produce results that are consistent with measured Hugoniot states. These simulations produce sharp shock fronts that are well described by traditional Hugoniot relations. Three-dimensional mesoscale simulations explicitly model the foam structure embedded with discrete platinum particles. The heterogeneous structure of the foam results in diffuse shock fronts and an unsteady post-shock state with large fluctuations about an average state. We will compare shock propagation through pure foam and Pt-doped foams at equal average initial density. Platinum-doped PMP foam experiments conducted at Sandia's Z facility provide data that can be used to test EOS mixing rules. We examine how well the results of the various chunk and atomic mix rules compare to the experimentally measured Hugoniot states.

2. Material models and EOS mixing rules

Reference [16] outlines the process by which PMP foams are manufactured. The Pt-doped PMP foams are manufactured in a similar manner except that a platinum powder, with sub-micron particle sizes, is added to the PMP/solvent solution to produce foams of nominally 0.300 g/cm^3 density and a 50-50 PMP/Pt mixture by weight. The mixtures are well stirred in an attempt to homogenize the foams. Figure 1 shows SEM images of pure and Pt-doped foams. In these samples the platinum particles coat the polymer fabric. Evidence of isolated particles, as well as clumping of the particles, is observed. We attempt to capture the gross features of these samples in the mesoscale simulations later in this report.

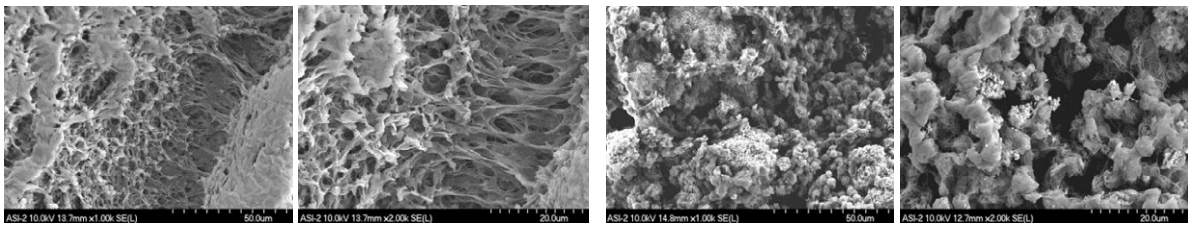

Pure 0.300 g/cm^3 foam Pt-doped 0.300 g/cm^3 foam

Fig. 1. Comparison of scanning electron microscope (SEM) images of pure and Pt-doped foams at nominally 0.300 g/cm^3 density. Foam samples were broken in half and then sputtered with a thin layer of gold to facilitate SEM imaging. Images were taken at 50, 20 and 10 μm resolution. Only the 50 and 20 μm resolution images are shown.

Since tabular equations of state are not available for PMP, we substitute Los Alamos Sesame EOS 7171 for polyethylene as a surrogate. This is an EOS for branched (low-density) polyethylene [22,23]. The table does not explicitly treat polyethylene as a polymer, i.e. the EOS model used an average atom with atomic number of 8/3 and mass of 4.6757; however, since experimental data are used in the model, the polymeric nature is implicitly included in parts of the EOS. The EOS has a tension region and van der Waals loops in expansion. Hugoniot data are reproduced very well by this EOS because the data were used in the construction of this table. Our prior work has shown this EOS models well the shock data for full density PMP and polyethylene, as well as the pure foam densities [16,17]. For the homogenized ALEGRA simulations described later, the PMP foam model utilizes the P-α model which accounts for voids in the porous material through a distention parameter, $\alpha = \rho_{solid} / \rho$, the ratio of the material's solid density to the average porous density [16,17]. Similar EOS substitution was used in modeling laser-driven shocks in very low density PMP and TMPTA foams [24,25,26].

We use Sesame EOS 3730 for the platinum dopant [23] and Sesame EOS 7360 for the quartz window [27] that is included in the simulations. Sesame 3730 for platinum has a tension region and Maxwell constructions in the vapor dome. The model is stated to reproduce the experimental Hugoniot, zero-pressure density and bulk modulus, but also carries the warning that the EOS is not generally intended for the hot, expanded liquid-metal region. The table does not explicitly

include a melting transition. Sesame 7360 for quartz has a realistic treatment of the phase transitions, including melting and dissociation. It is stated to give very good agreement with the Hugoniot data up 600 GPa. Accurate treatment of quartz should include material strength. A yield strength of 4.8 GPa, shear modulus of 40.5 GPa, Poisson's ratio of 0.105, and melting temperature of ~2000 K is recommended in the model description.

2.1. Multi-material mixing rules

Many hydrodynamics codes such as ALEGRA and KULL do not use a single composite EOS for the evaluation of the state of a mixture. Instead, the physics algorithms combine the individual material EOS of the multiple materials that are present within a mesh element to determine the averaged material properties that affect the evolution of the physics. Thus, mixing rules apply whenever two or more materials are present within a single computational mesh element (or cell or zone). Multiple methods exist for modeling mixed materials and mixed equations of state in hydrodynamics codes. So-called chunk mix methods treat materials as immiscible substances that coexist in computational cells and employ various weighting techniques for computing the average material properties. Other atomic mix methods envision that materials are intimately mixed at the atomic level and average the equations of state that are then applied to the mixture. Evaporation models allow hydrodynamic simulations to transition between the two multi-material mix methods.

Material averaging usually involves the volume fractions, f_m, of the various materials present. One complete set of mixing formulas which is used by ALEGRA to compute average material properties is listed here [20,28].

$$
\begin{aligned}
1 &= \sum_m f_m & \bar{T} &= \sum_m \left(f_m \rho_m C_{v,m} T_m \right) \Big/ \left(\bar{\rho} \bar{C}_v \right) & \bar{P} &= \bar{K} \cdot \sum_m \left(f_m P_m / K_m \right) \\
\bar{\rho} &= \sum_m \left(f_m \rho_m \right) & \bar{C}_v &= \sum_m \left(f_m \rho_m C_{v,m} \right) \Big/ \bar{\rho} & 1/\bar{K} &= \sum_m \left(f_m / K_m \right) \\
\bar{e} &= \sum_m \left(f_m \rho_m e_m \right) \Big/ \bar{\rho} & \bar{k} &= \sum_m \left(f_m k_m \right) & \bar{\sigma}_a &= \sum_m \left(f_m \sigma_{a,m} \right)
\end{aligned}
\qquad (1)
$$

where ρ_m is the density, e_m is the specific internal energy, T_m is the temperature, $C_{v,m}$ is the specific heat, k_m is the thermal conductivity, P_m is the pressure, and K_m is the bulk modulus. $\sigma_{a,m}$ is the radiation absorption coefficient and the rule is for atomically mixed materials; for chunk mix the inverse coefficients are averaged similar to the bulk modulus [3,4]. The material parameters, *e.g.*, ρ_m, T_m, etc., are normal values within the volume fraction the material occupies. They are not renormalized in any way. Thus equations of state and other material models may be called with normal densities and temperatures, etc. For example, the EOS for material m is evaluated as $e_m = e_m(\rho_m, T_m)$ and $P_m = P_m(\rho_m, T_m)$. These averaging equations are rooted in expressions for the conservation of volume, mass, and energy. The exception may be the averaging expression for the pressure. Other codes and methods may have alternate formulas for computing average material properties. We focus on the treatment of the average pressure in the subsections that follow.

2.2. Constant volume fraction algorithm (ALEGRA and KULL)

A legacy algorithm found in ALEGRA and KULL assumes that the volume fractions, f_m, remain constant as a mesh element compresses or expands. There is no pressure or temperature equilibration of the materials within the mesh element. All materials experience the same relative volume change and $f_{m,new} = f_{m,old}$. Under this algorithm the new density and specific energy are computed as:

$$
\begin{aligned}
\rho_{m,new} &= \rho_{m,old} \cdot \left(V_{old} / V_{new} \right) \\
e_{m,new} &= e_{m,old} \cdot \left(\rho_{m,old} V_{old} / \rho_{m,new} V_{new} \right)
\end{aligned}
\qquad (2)
$$

where V_{old} and V_{new} are the old and new cell volumes before and after cell compression or expansion. The volume fractions drop out of the expressions for the density and specific internal energy. Note we do not address here the additional energy changes due to $P \cdot dV$ work, external forces, or other physics algorithms, such as thermal conduction, Joule heating, or radiative emission or absorption. Once the new densities and specific internal energies are known, then the EOS models are updated to determine new temperatures, and then new pressures, consistent with the updated densities and specific internal energies. The constant volume fraction algorithm also uses a simplistic method to compute the average material pressure using only the volume fractions to weight the individual material pressures.

$$\bar{P} = \sum_m f_m P_m \tag{3}$$

There are substantial drawbacks to the constant volume fraction algorithm. While pressures and temperatures may equilibrate with neighboring mesh cells, there is usually no mechanism for the pressures and temperatures to equilibrate among the materials present within the same mesh element. This leads to unphysically high pressure and temperature states for stiff materials under extreme loading conditions, especially for solid materials, and pressure differences of a few to several orders of magnitude are observed. The equality of the pressures and particle velocities of materials in contact with one another is a fundamental property of shock dynamics, and this property is violated.

2.3. Isentropic multi-material algorithm (ALEGRA) or mixed-zone multi-material algorithm (KULL)

The isentropic multi-material (IMM) algorithm in ALEGRA accounts for the relative stiffness of the multiple materials in a mesh element [20,29]. The equivalent method in KULL is mixed-zone multi-material algorithm [30,31]. The pressure average is bulk modulus weighted as in Eq. (1), although KULL uses volume fraction weighting in expansion as in Eq. (3). These algorithms are sometimes referred to as pressure relaxation or chunk mix methods. The bulk modulus for a material is defined from the variation of pressure with the specific volume.

$$K_m = -v_m \frac{\partial P_m}{\partial v_m} = \rho_m \frac{\partial P_m}{\partial \rho_m} \approx \rho_m C_{s,m}^2 \tag{4}$$

where $v_m = 1/\rho_m$ is the specific volume and $C_{s,m}$ is the sound speed. This method usually has a mechanism by which the individual pressures are equilibrated among the materials to the average element pressure by evolving the volume fractions (and hence densities) of the constituent materials. The method may also include temperature equilibration among the constituent materials, either by a radiative transfer model [29] or by a thermal conduction model over a thermal timescale given by $\tau_{thermal} = \left(l^2 \bar{\rho} \bar{C}_v\right) / \bar{k}$ where l is a characteristic cell size and $\bar{k}$ is the thermal conductivity [28].

2.4. Atomic mix multi-material algorithm (KULL)

For high temperatures, materials transition to an atomic state or plasma, and materials become intimately mixed at the atomic level [32]. In this case, it is more convenient to combine EOS according to the mass fractions y_m of the materials rather than the volume fractions f_m, however the two are related by $y_m = f_m \cdot \left(\rho_m / \bar{\rho}\right)$. Mass fractions remain constant as materials equilibrate, whereas the volume fractions do not. The atomic mix rule tacitly assumes pressure equilibrium among the constituent materials. Individual densities ρ_m (or specific volumes v_m) are adjusted by a Newton-Raphson procedure to equilibrate the pressures, and importantly are constrained to conserve mass, or equivalently the mean mixture density or the mean specific volume.

$$\bar{v} = \frac{V}{M} = \sum_m \frac{f_m V}{M} = \sum_m \frac{f_m \rho_m}{\bar{\rho}} \cdot \frac{1}{\rho_m} = \sum_m y_m v_m \qquad \text{differentiation leads to} \qquad 1 = \sum_m y_m \frac{\partial v_m}{\partial \bar{v}} \tag{5}$$

where V and M are the total cell volume and mass. The average pressure is computed according to the weights from Eq (5):

$$\bar{P} = \sum_m y_m \frac{\partial v_m}{\partial \bar{v}} P_m \tag{6}$$

The average specific internal energy is $\bar{e} = \sum_m y_m e_m$ which actually is a rewrite from Eq. (1). While the KULL user may choose to equilibrate the atomic mix rule according to alternate variables such as the chemical potential or the analytic or tabular electron density, only pressure equilibration is considered here. Pressure equilibration is the only variable that maintains thermodynamic consistency [32].

3. Quasi-1D simulations of Pt-doped PMP foams

In this section we report on two sets of homogenized, one-dimensional simulations of doped PMP foams. The first set are idealized Noh-type simulations where the homogenized foam impacts a perfectly rigid wall to ascertain trends, similarities and differences in the various mixing rules as the impact speed and initial average density of the foam are varied. The second set of simulations are customized 1D simulations that impact a homogenized stationary foam with realistic aluminum flyer plate profiles from MHD simulations and are tailored for direct comparison to experiment.

The composition of doped foams is typically specified by the mass fraction of each constituent, such as a 50-50 mixture by weight. However, the parameters that are needed to initialize simulations are the material volume fractions. Given the desired average foam density, ρ_{doped} (0.300 g/cm^3), the density of solid platinum, ρ_{Pt} (21.45 g/cm^3), and mass fractions of PMP and platinum, y_{PMP} and y_{Pt} (0.50 each), one may compute the volume fractions of the two materials as well as the average density of just the PMP component, ρ_{PMP}, from the volume fraction and density relations in Eq. (1).

$$f_{Pt} = y_{Pt}\left(\rho_{doped}/\rho_{Pt}\right) \qquad f_{PMP} = 1 - f_{Pt} \qquad \rho_{PMP} = \rho_{doped}\left(y_{PMP}/f_{PMP}\right) \tag{7}$$

For example, with the above values for doped foam density, platinum density, and mass fractions, $f_{Pt} = 0.006993$, $f_{PMP} = 0.993007$, and $\rho_{PMP} = 0.1511$ g/cm^3. So while the PMP and the platinum have equal mass fractions, the platinum is only a small fraction of the volume of the doped foam due to the large density differences.

3.1. One-dimensional Noh-type planar shock simulations

Planar Noh-type [33] foam simulations are studied for Pt-doped foams in a manner similar to the pure foam simulations in Reference [17]. Homogenized, quasi-1D ALEGRA and KULL simulations model the idealized constant-velocity, piston-driven shock problem which is the basis for deriving the traditional Hugoniot jump conditions [34,35]. These simulations initialize every mesh element with PMP and platinum according to the volume fractions and densities defined by Eq. (7). Average initial doped foam densities are chosen to be 0.200, 0.300, and 0.400 g/cm^3. A series of 15 simulations with 15 different velocities were performed for each foam density and each EOS mixing rule. The velocities start at 2 km/s, then range to 30 km/s by 2 km/s increments. The results are shown in Figure 2.

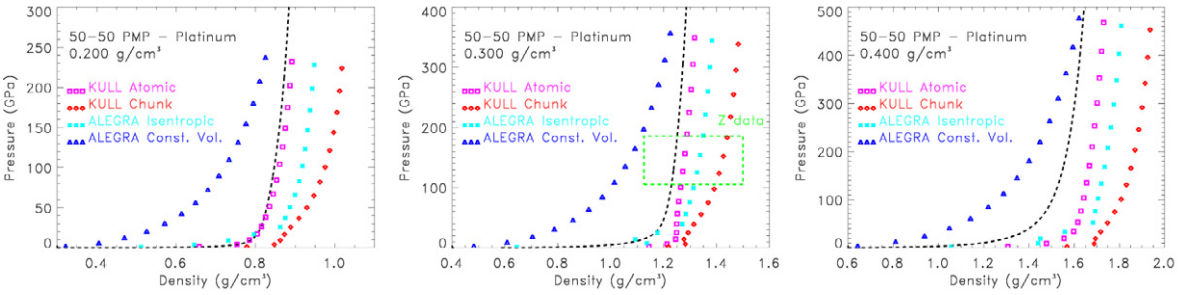

Fig. 2. Comparison of doped foam Hugoniot curves at three densities, 0.200, 0.300 and 0.400 g/cm^3, for four EOS mixing rules. The analytic pure foam Hugoniots (dashed lines) are superimposed on the doped foam simulation data. This shows the close proximity of pure and doped foam Hugoniot curves due to conservation of mass, momentum and energy. This also indicates the ranges of the Hugoniot densities and pressures to be expected as one varies the mass fraction of the platinum from 0 to 0.5. The approximate range of Z experimental data is indicated in the plot for 0.300 g/cm^3 foam.

Hugoniot relations are based upon conservation of mass, momentum and energy. In order to solve completely for the Hugoniot state, closure of the equations with an EOS model is necessary, thus the various EOS mixing rules lead to different Hugoniot curves as can be seen in Fig. 2. The legacy constant volume fraction algorithm leads to significantly higher pressures at lower densities than the other models due to over compression of the solid platinum. This Hugoniot does not pass through the region of experimental data for 0.300 g/cm^3, clearly showing this rule to be an inaccurate rule. ALEGRA's insentropic bulk-modulus weighted (chunk mix) and KULL's atomic mix rules are much closer together, and both of these curves pass through the center of the range of Z experimental data. KULL's bulk-modulus weighted, chunk mix rule results in the softest Hugoniot and has the highest density for any given pressure. Therefore, both ALEGRA's isentropic multi-material model and KULL's atomic mix rule may be considered valid models within the scope of this work.

Table 1: Summary of experimental and simulated shocked Pt-doped foam results

Z shot	Foam density (g/cm^3)	Flyer velocity (km/s)	Experimental density (g/cm^3)	Simulation density (g/cm^3)	Experimental pressure (GPa)	Simulation pressure (GPa)
1911 N2	0.279	20.58	1.126 ± 0.058	1.217 ± 0.012	105.95 ± 2.95	102.40 ± 1.25
1911 N4	0.292	20.58	1.144 ± 0.032	1.269 ± 0.013	110.46 ± 0.83	106.10 ± 1.37
1911 S2	0.295	22.26	1.128 ± 0.049	1.286 ± 0.014	129.69 ± 1.56	123.17 ± 2.02
1911 S4	0.300	22.26	1.339 ± 0.145	1.306 ± 0.015	126.84 ± 3.32	124.76 ± 2.07
1912 N2	0.300	24.17	1.49 ± 0.166	1.312 ± 0.017	144.66 ± 3.49	144.90 ± 2.86
1912 N4	0.306	24.17	1.229 ± 0.125	1.336 ± 0.018	153.87 ± 5.01	147.08 ± 2.96
1912 S2	0.313	25.63	1.24 ± 0.056	1.370 ± 0.019	174.76 ± 5.77	166.69 ± 3.59
1912 S4	0.332	25.63	1.219 ± 0.093	1.444 ± 0.021	186.33 ± 11.23	174.16 ± 3.95

3.2. Customized simulations of Pt-doped PMP foam experiments

To select which EOS mixing rule is the most accurate, we use experiments to verify the simulation results. A set of eight Pt-doped foam experiments were shot at Sandia's Z facility. The data were taken on Z shots 1911 and 1912. The average density of the foam samples was 302.125±14.675 mg/cm^3. Magnetically driven flyer impact velocities ranged from 20.6 to 25.6 km/s. The results from a preliminary analysis of the experimental data are given in Table 1.

Customized quasi-1D simulations are compared to this experimental data. The hydrodynamic impact simulations are initialized with aluminum flyer density, temperature and velocity profiles computed in separate MHD simulations of Z shot 1910. The flyer profiles are representative of the flyer state at the time of impact. The flyer profiles are shown in Figure 3. Approximately 100 μm of the originally 900 μm thick flyer is still in the solid state. The amplitude of the flyer velocity profile is scaled for each simulation to match the unfolded experimental flyer velocity. The simulated foam density is adjusted to match the measured initial sample foam density. The results of the simulations also are shown in Figure 3 and listed in Table 1.

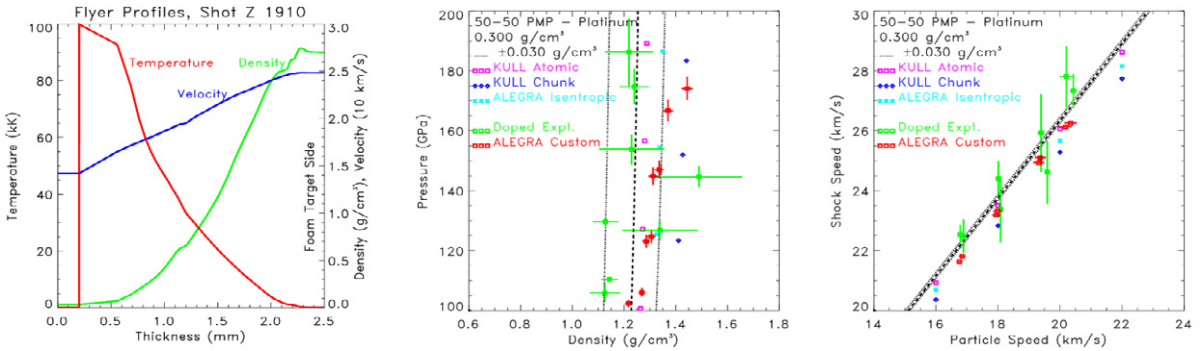

Fig. 3. (Left) Aluminum flyer profiles for customized Pt-doped foam simulations. The flyer moves to the right and impacts a sample of foam located to the right. MHD flyer profiles courtesy of R. W. Lemke, SNL. (Middle) Overlay of Pt-doped foam experimental data (green squares), customized simulation data (red squares), Noh-type simulation data (magenta, cyan and blue points without error bars), and analytic pure foam Hugoniot data in the *P*-ρ plane (dashed and dotted lines). (Right) The same experimental and simulation data plotted in the Us-Up plane.

Figure 3 shows that the customized ALEGRA simulations using ALEGRA's bulk-modulus weighted, isentropic multi-material algorithm lie within the range of Z experimental data supporting the prior assertion that this algorithm is a valid pressure mixing rule. Data from the various Noh-type simulations are also superimposed. The custom and Noh-type ALEGRA simulation data are consistent with each other, demonstrating the validity of Noh-type simulations. Because the simulation data from the KULL atomic mixing algorithm also passes cleanly through the experimental data, this algorithm also is determined to be a valid pressure mixing rule. The KULL chunk mixing algorithm lies significantly away from the experimental data (~10%), so this mixing algorithm is concluded to be less precise for this application.

4. Three-dimensional mesoscale shock simulations

3D mesoscale simulations attempt to capture the truly 3D structure of the doped plastic foams. Whereas quasi-1D simulations only represent uniaxial motion and uniaxial strains, 3D mesoscale simulation allow transverse motions and transverse strains. The mesoscale simulations are conducted using ALEGRA, and the isentropic multi-material mixing rule, because this code allows doubly periodic meshes in the transverse directions and does not inhibit transverse motions. Material exiting one face of the mesh reenters the opposite periodic face. Simulations with no displacement (fixed or mirror) boundary conditions on the side faces inhibit transverse motion.

Initial foam conditions are based upon the SEM images of the foam shown previously in Figure 1. A representative initial state for the mesoscale simulations is depicted in the unshocked state of Figure 5. We model a foam sample with dimensions 200×48×48 microns. The simulations presented here use 0.4 micron mesh resolution leading to 7.2 million mesh elements in the foam. This resolution is marginal at best and higher resolution simulations at 0.2 and 0.1 micron cell size are in progress (however those simulations have not yet progressed sufficiently to yield significant results for this report). The simulations use arbitrary-Lagrangian-Eulerian (ALE) meshes, therefore all the foam mesh elements remain in the foam and the full resolution in terms of number of mesh elements is retained.

The doped foam is represented by a combination of hollow PMP spheres, with flat platinum disks for the dopant. Spheres and disks are inserted into the simulation until the correct average density of each material is achieved according to the formulae in Eq. 7. Hollow spheres of PMP are randomly located in the mesh. The outer radii of the spheres are varied between 1 and 5 microns and the wall thicknesses between 0.5 and 1 micron. Flat disks of platinum are also randomly located and randomly oriented. The radii of the disks are varied between 1 and 5 microns and the disk thicknesses between 0.5 and 1 microns. Figure 4 shows the platinum disks with the visualization of the PMP supressed. A portion of a quartz window moving at the same initial speed as the foam bounds the foam on the right hand side.

Figure 5 shows a suite of density, temperature and pressure snapshots for the 0.300 g/cm^3 doped foam sample impacting a virtual rigid wall at 20 km/s. The impact produces a hot low-density mixed PMP-Pt vapor that streams through the voids of the foam, and when averaged with the intact foam, results in a diffuse shock front as shown in Figure 6. The shock front moves through the foam at a fairly constant velocity that matches the 1D shock velocity. The PMP foam shells and Pt disks persist within the low-density vapor until vaporized and absorbed into the shocked material. Lines superimposed on Figures 4 and 5 denote planes at 20 micron intervals into the foam.

The state of the platinum dopant is easily hidden by the vaporized PMP, therefore we illustrate the vaporization and mixing of the platinum dopant with the PMP vapor in Figure 4. The solid PMP and solid platinum are shock heated to vaporization and ionization, producing a turbulent post-shock state. The mixed vapor exhibits high vorticity and random fluctuations in density, temperature and pressure that traverse the shock material in all directions. Direct numerical simulation of this turbulence mixes the PMP and platinum so that the post-shock state trends toward the mixed state of the quasi-1D simulations, implying that conclusions learned there are applicable here, namely that the chunk and atomic mixing rules are valid here.

Renderings of the 3D mesoscale simulations produce results that are qualitative and are hard to compare directly with experiment and 1D simulation results. A post-processing code was written to compute mean and root-mean-square (RMS) values of simulated quantities by simple averaging over the transverse planes of the simulation, thereby producing lineouts as a function of depth into the foam. Density, temperature and pressure lineouts and RMS deviations are shown at 3 simulation times in Figure 6. Large density variations are present in initial conditions of the foam due to the randomness of the PMP spheres, Pt disks and voids. The initial temperature and pressure randomness are small in magnitude relative to the post-shock state and cannot be seen in the temperature and pressure lineouts.

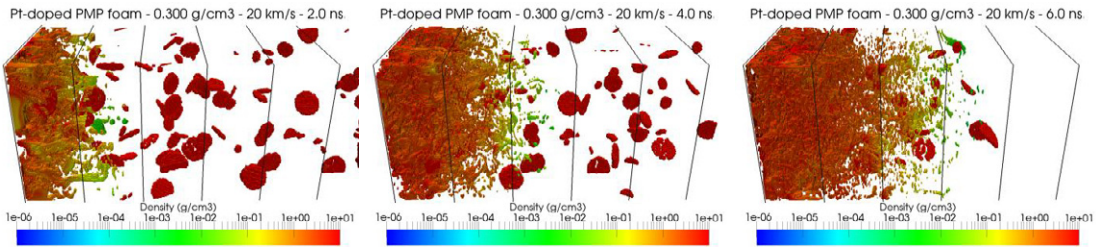

Fig. 4. Snapshots of the state of the platinum dopant with the PMP not visualized and at times 2, 4 and 6 ns. The 20 km/s impact with a virtual rigid wall is sufficient to vaporize both the PMP foam and the platinum dopant. Solid disks of Pt move toward the left while vaporized Pt mixes and expands toward the right. Turbulence seeded by the random foam initial state mixes the vaporized materials. Lines denote planes at 20 micron intervals into the foam.

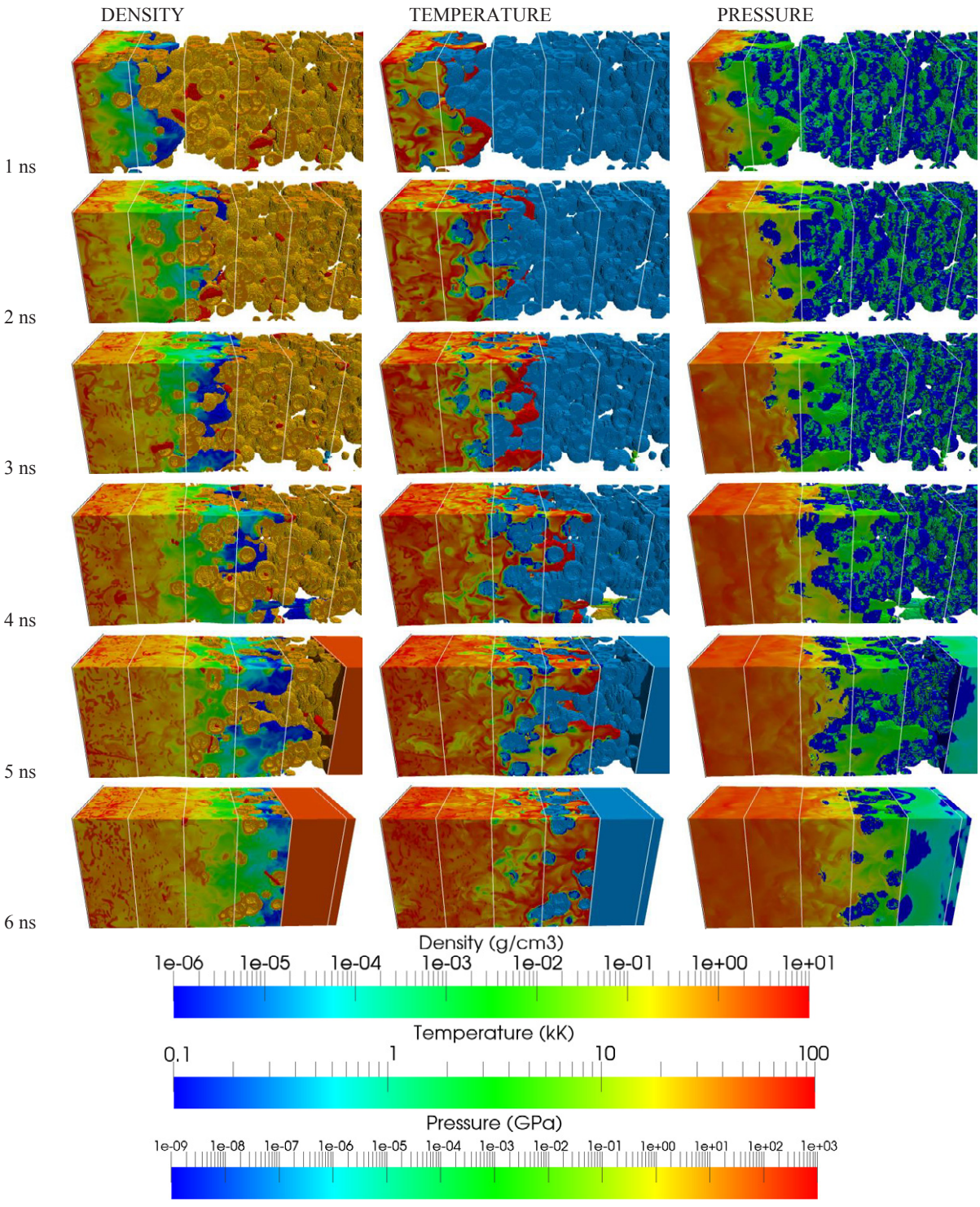

Fig. 5. Density, temperature and pressure snapshots for a 300 mg/cm^3, 200×48×48 micron, doped foam sample impacting a rigid wall at the left hand side at 20 km/s from 3D ALEGRA mesoscale simulation. The impact produces a hot low-density mixed PMP-Pt vapor that streams through the voids of the foam, and when averaged with the intact foam results in a diffuse shock front. The foam-void initial condition persists within this vapor until absorbed into the shocked material. A quartz window bounds the foam on the right hand side. White lines denote planes at 20 micron intervals into the foam.

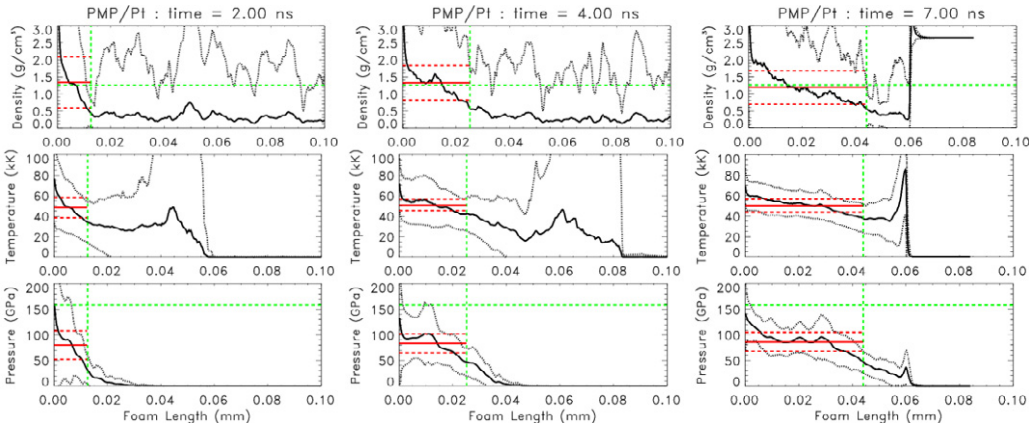

Fig. 6. Lineouts of the mean density, temperature and pressure profiles averaged over the transverse planes of Fig. 5. Both mean (black solid lines) and RMS deviations (black dotted lines) are plotted as a function of depth into the foam. Superimposed on the lineouts are the 1D shock location (vertical green dash line) and the 1D Hugoniot values for density and pressure (horizontal green dash lines). Also shown are the global mean and RMS density, temperature, and pressure for the volume defined by the 1D shock location (horizontal red solid and dashed lines). The quartz window is seen in the density and temperature plots at 7 ns.

A sharp shock front is absent in the averaged density, temperature and pressure profiles of Figure 6. Instead the average of the vapor and the solid produces a diffuse profile. The 1D shock location empirically seems to be coincident with the location at which the density and pressure are above one half the average of the post-shock states. The vaporized material produces a foot that extends ahead of the 1D shock location. The expansion of the hot, low-density vapor is clearly evident in the temperature profiles. The hot vapor and the foot material softens the impact of subsequent material and causes the post-shock pressure to be significantly lower than the pressure computed by 1D simulation and 1D analysis of experiment. The RMS uncertainties in the 3D mesoscale simulations are greater than the reported experimental errors. Smaller experimental error bars are due in large part to the assumption of 1D-like behavior in the analysis of the experimental results. It is not clear at present how 3D effects can be factored into the experimental analysis.

Because 3D mesoscale simulations permit transverse motion in addition to gradual compaction, more of the energy remains in the form of kinetic energy and less as internal energy. A comparison of the energy tallies between the 1D and 3D simulations is shown in Figure 7. The left-most plot shows the conversion of kinetic energy into internal energy as the foam impacts the rigid boundary. The 1D simulation has excellent energy conservation, whereas the 3D simulation suffers numerically from a 16% energy loss. The right-most plot rescales the 3D energy tallies to emulate zero numerical energy loss. In both of these plots it is clear that the 3D kinetic energy remains above the 1D kinetic energy by 33% to 50% due to transverse motion. The 3D internal energy remains below the 1D internal energy contributing to the lower pressure in the 3D simulations.

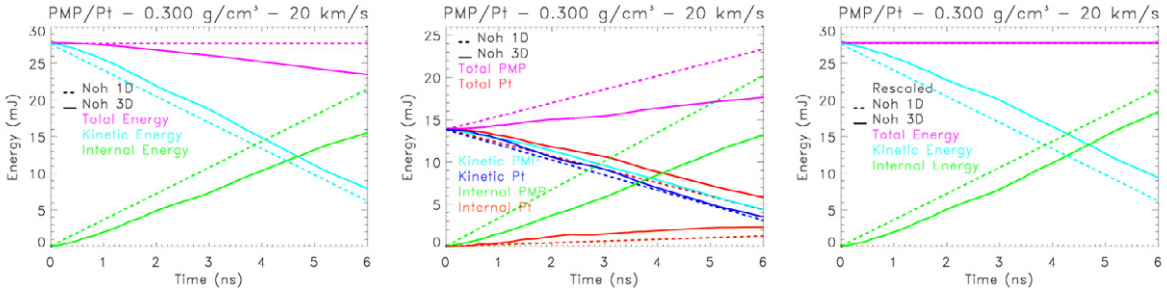

Fig. 7. Comparison of total, kinetic and internal energies from 1D simulation (dashed lines) and 3D simulation (solid lines). (Left) Total, kinetic and internal energy tallies show the conversion of kinetic into internal energy, as well as a 16% energy loss in the 3D simulation. (Middle) Break down of the total, kinetic and internal energies by material. (Right) Energy tallies from the left plot renormalized to emulate no numerical energy loss.

The middle plot of Figure 7 illustrates the energy partitioning between the PMP and the platinum. Both the PMP and the platinum start with the same kinetic energy due to the fact that this is a 50-50 mixture by weight. Both the PMP and the platinum lose kinetic energy at the same rate, and the rate is about the same in both 1D and 3D simulations. The lost kinetic energy predominantly goes into the PMP internal energy and to a lesser extent into the platinum internal energy. The largest energy discrepancy between the 1D and 3D simulation is in the PMP internal energy. Even if all of the lost energy would have been manifested as internal energy of the PMP or Pt, this would not increase the 3D pressure up to 1D or experimental pressures.

The start of shock compression of the quartz window to 3.2 g/cm^3 is evident at 7 ns in Figure 6. A reflected shock returning into the foam from the foam-quartz interface also is seen in the temperature and pressure profiles. The 3D mesoscale simulation terminates shortly after this time due to mesh instabilities at the foam-quartz interface. Figure 8 shows buckling of the quartz window face and the non-uniformity of the shock as it enters the quartz at 7 ns simulation time. This non-uniformity is consistent with the disruption of the VISAR signal seen in the experiments that defines the shock transit time through the foam. The computed shock speed from the simulation is 28.57 km/s. The experimental shock speed for a 20.4 km/s flyer impact is measured to be 27.8±1.0 km/s.

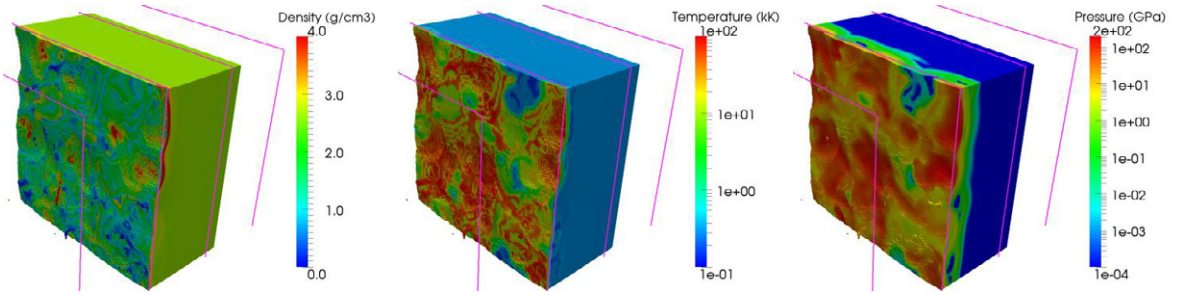

Fig. 8. Buckling of the quartz window face and the non-uniformity of the shock entering the quartz at 7.0 ns. Visualization of the foam is suppressed. The initial quartz density is 2.648 g/cm^3 implying significant compression of the quartz is beginning.

5. Conclusion

We have used two state-of-the-art simulation codes, ALEGRA and KULL, to examine the validity of four EOS mixing rules. Through comparison of quasi-1D modeling to experiment we have demonstrated the inaccuracy of the legacy constant volume fraction mixing rule, and also established the suitability of ALEGRA's bulk-modulus weighted, isentropic (chunk mix) mixing rule, as well the suitability of KULL's atomic mixing rule, to model shock compressed platinum-doped foams. Through 3D mesoscale simulation we have shown that shock compression of foam is a complex process, and that quasi-1D simulation and experimental analysis may over simplify the model of shocked foams.

Acknowledgements

The authors thank Analytical Solutions, Inc., Albuquerque, NM for performing the SEM analysis shown in this report. We also thank the ALEGRA and KULL code development teams for provided the computational tools for these simulations. The 1D ALEGRA and KULL simulations were run on the ASC TLCC Glory computing platform, and the 3D ALEGRA mesoscale simulations were run on the ASC TLCC2 Chama computing platform, both located at Sandia National Laboratories. Higher resolution simulations are in progress on the ASC Cielo supercomputer located at Los Alamos National Laboratory. Sandia National Laboratories is a multi-program laboratory managed and operated by Sandia Corporation, a wholly owned subsidiary of Lockheed Martin Corporation, for the U.S. Department of Energy's National Nuclear Security Administration under contract DE-AC04-94AL85000.

References

[1] Wilson, D.C., Ebey, P.S., Sangster, T.C., *et al.*, 2011. "Atomic mix in directly driven inertial confinement implosions," Phys. Plasmas, 18, p. 112707.
[2] Hammel, B.A., Scott, H.A., Regan, S.P., *et al.*, 2011. "Diagnosing and contolling mix in National Ignition Facility implosion experiments," Phys. Plasmas, 18, p. 056310.

[3] Prinja, A.K. and Olson, G.L., 2005. "Grey radiative transfer in binary statistical media with material temperature coupling: asymptotic limits," JQSRT, 90 (2) pp. 131-159.
[4] Smith, C.C., 2003. "Opacity consideration for an experiment to measure radiation flow in an inhomogeneous binary mixture," JQSRT, 81 (1-4) pp. 451-459.
[5] Horner, D.A., Kress, J.D. and Collins, L.A., 2010. "Effects of metal impurities on the optical properties of polyethylene in the warm dense-matter regime," Phys. Rev. B, 81, p. 214301.
[6] Chang, C.H., and Ramshaw, J.D., 2005. "Pressure force transition and mixture morphology evolution in heterogeneous mixtures," Theor. Comput. Fluid Dyn., 19 (4) pp. 253-260.
[7] Alfe, D., Gillan, M.J. and Price, G.D., 2002. "*Ab initio* chemical potentials of solid and liquid solutions and the chemistry of the Earth's core," J. Chem. Phys., 116 (16) pp. 7127-7136.
[8] Ostanin, S., Alfe, D., Dobson, D, *et al.*, 2006. "*Ab initio* study of the phase separation of argon in molten iron at high pressures," Geophys. Res. Lett., 33, p. L06303.
[9] Lorenzen, W., Holst, B. and Redmer, R., 2009. "Demixing of hydrogen and helium at Megabar pressure," Phys. Rev. Lett., 102, p. 115701.
[10] Wilson, H.F. and Militzer, B., 2010. "Sequestration of Noble Gases in Giant Planet Interiors," Phys. Rev. Lett., 104, p. 121101.
[11] Dai, J.D., Hou, Y. and Yuan, J., 2010. "Quantum Langevin Molecular Dynamic Determination of the Solar-Interior Equation of State," Astro. J., 721, pp. 1158-1163.
[12] Magyar, R.J., Root, S., Haill, T.A., *et al.*, 2012. "Equations of State of Mixtures: Density Functional Theory (DFT): Simulations and Experiments on Sandia's Z Machine," in Shock Compression of Condensed Matter-2011, American Institute of Physics, 1426, pp. 1195-1198.
[13] Magyar, R.J., Root, S., Mattsson, T.R. and Cochrane, K., 2012. "Ethane and xenon mixing: density functional theory (DFT) simulations and experiments on Sandia's Z machine," Technical report SAND2012-1942C, Sandia National Laboratories, Albuquerque, NM, March 2012 (presented at the American Physical Society March Meeting 2012, Boston, MA.).
[14] Mattsson, T.R., Lane, J.D.M., Cochrane, K.R., *et al.*, 2010. First-principles and classical molecular dynamics simulation of shocked polymers, Phys. Rev. B, 81, p. 054103.
[15] Cochrane, K.R., Desjarlais, M.P. and Mattsson, T.R., 2012. "Density Functional Theory (DFT) Simulations of Polyethylene: Principal Hugoniot, Specific Heats, Compression and Release Isentropes," in Shock Compression of Condensed Matter, American Institute of Physics, 4126, pp. 1271-1274.
[16] Root, S., Haill, T.A., Lane, J.D.M., *et al.*, 2012. Shock compression of hydrocarbon foam to 200 GPa: experiment, mesoscale modeling and atomistic simulations, J. Appl. Phys., submitted.
[17] Haill, T.A., Mattsson, T.R., Root, S., *et al.*, 2012. "Mesoscale Simulation of Shocked Poly-(4-Methyl-1-Pentene) (PMP) Foams," in Shock Compression of Condensed Matter, American Institute of Physics, 1426, pp. 913-916.
[18] Lane, J.M.D., Grest, G.S., Thompson, A.P., *et al.*, 2012. "Shock Compression of Hydrocarbon Polymer Foam Using Molecular Dynamics," in Shock Compression of Condensed Matter, American Institute of Physics, 1426, pp. 1435-1438.
[19] Summers, R.M., Peery, J.S., Wong, M.K., *et al.*, 1997. Recent Progress in ALEGRA Development and Application to Ballistic Impacts, Int. J. Impact Engng., 20, p. 779-788.
[20] Robinson, A.C., Brunner, T.A., Carroll, S., *et al.*, 2008. "ALEGRA: An Arbitrary Lagrangian-Eulerian Multimaterial, Multiphysics Code," Proceedings of the 46th AIAA Aerospace Science Meeting and Exhibit, American Institute of Aeronautics and Astronautics, AIAA 2008-1235.
[21] Rathkopf, J.A., Miller, D.S., Owen, J.M., *et al.*, 2000. "KULL: LLNL's ASCI Inertial Confinement Fusion Simulation Code," Proceedings of the PHYSOR2000: ANS International Topical Meeting on Physics and Mathematics and Computation into the Next Millennium, American Nuclear Society. (Also available as Technical Report UCRL-JC-137053, Lawrence Livermore National Laboratories, Livermore, CA, February 2000.)
[22] Dowell, F., 1982. "A Simple EOS for Branched (Low-Density) Polyethylene," Technical report LA-9559-MS, Los Alamos National Laboratory, Los Alamos, NM, October 1982.
[23] Holian, K.S., 1984. "T-1 Handbook of Material Properties Data Bases: Vol. 1c, Equations of State," Technical report LA-10160-MS, Los Alamos National Laboratory, Los Alamos, NM, November 1984.
[24] Dezulian, R., Canova, F., Barbanotti, S., *et al*., 2006. "Hugoniot data of plastic foams obtained from laser driven shocks," Phys. Rev. E, 73, p. 047401.
[25] Koenig, M., Benuzzi, A., Philippe, F., *et al*., "Equation of state data experiments for plastic foams using smoothed laser beams," Phys. Plasmas, 6 (8), pp. 3296-3301.
[26] Hall, T., Batani, D., Nazarov, W., *et al*., 2002. "Recent advances in laser-plasma experiments using foams," Laser Part. Beams, 20, pp. 303-316.
[27] Kerley, G.I., 1999. "Equations of State for Composite Materials," Technical report KPS99-4, Kerley Publishing Services, Albuquerque, NM, December 1999.
[28] Brunner, T.A., Haill, T.A., Robinson, A.C., and Wong, M.K., 2004. "Multi-Material Treatment in ALEGRA," Unpublished report, Sandia National Laboratories, Albuquerque, NM, November 2004.
[29] Rider, W. and Love, E., 2009. "Mutimaterial Treatment," Unpublished report, Sandia National Laboratories, Albuquerque, NM, June 2009.
[30] Miller, D.S., Zimmerman, G.B., 2007. "An Algorithm for Time Evolving Volume Fractions in Mixed Zones in Lagrangian Hydrodynamics Calculations," Numerical Methods for Multi-Material Fluid Flows (MULTIMAT 2007), Czech Technical University, Prague, Czechoslovakia, http://www-troja.fjfi.cvut.cz/~multimat07/.
[31] Anninos, P., 2002. Kull ALE: I. Unstructured Mesh Advection, Interface Capturing, and Multiphase 2T RHD with Material Interfaces, Technical Report UCRL-ID-147297-PT-1, Lawrence Livermore National Laboratories, Livermore, CA, February 2002.
[32] Ulitsky, M., Zimmerman, G., Renard, P., 2006. Combining Equations of State in Kull, Technical Report UCRL-TR-224230, Lawrence Livermore National Laboratories, Livermore, CA, September 2006.
[33] Noh, W.F., 1978. "Errors for Calculations of Strong Shocks Using an Artificial Viscosity and an Artificial Heat Flux", J. Comp. Phys., 72, pp. 78-120.
[34] Zel'dovich, Y.B. and Raizer, Y.P., 1966. Physics of Shock Waves and High-Temperature Hydrodynamics Phenomena, Academic Press, New York.
[35] Asay, J.R. and Shahinpoor, M., 1993. High-Pressure Shock Compression of Solids, Springer-Verlag, New York.